Anatomic Localization of Rapid Repetitive Sources in Persistent Atrial Fibrillation

Fusion of Biatrial CT Images With Wave Similarity/Cycle Length Maps

Flavia Ravelli, PhD,* Michela Masè, PhD,* Alessandro Cristoforetti, PhD,*
Maurizio Del Greco, MD,† Maurizio Centonze, MD,‡ Massimiliano Marini, MD,†
Marcello Disertori, MD†

Trento, Italy

OBJECTIVES The aim of this study was to investigate the anatomic distribution of critical sources in patients with atrial fibrillation (AF) by fusion of biatrial computed tomography (CT) images with cycle length (CL) and wave similarity (WS) maps.

BACKGROUND Experimental and clinical studies show that atrial fibrillation (AF) may originate from rapid and repetitive (RR) sources of activation. Localization of RR sources may be crucial for an effective ablation treatment. Atrial electrograms showing rapid and repetitive activations can be identified by combining WS and CL analysis.

METHODS Patients with persistent AF underwent biatrial electroanatomic mapping and pre-procedural CT cardiac imaging. WS and CL maps were constructed in 17 patients by calculating the degree of repetitiveness of activation waveforms (similarity index [S]) and the cycle length at each atrial site. WS/CL maps were then integrated with biatrial 3-dimensional CT reconstructions by a stochastic approach.

RESULTS Repetitive sources of activation (S ≥0.5) were present in most patients with persistent AF (94%) and were mainly located at the pulmonary veins (82% of patients), at the superior caval vein (41%), on the anterior wall of the right atrium (23%), and at the left atrial appendage (23%). Potential driver sources showing both rapid and repetitive activations (CL = 140.7 ± 25.1 ms, S = 0.65 ± 0.15) were present only in a subset of patients (65%) and were confined to the pulmonary vein region (47% of patients) and left atrial appendage (12%). Differently, the repetitive activity of the superior caval vein was characterized by a slow activation rate (CL = 184.7 ± 14.6 ms).

CONCLUSIONS The identification and localization of RR sources is feasible by fusion of biatrial anatomic images with WS/CL maps. Potential driver sources are present only in a subset of patients with persistent AF and are mainly located in the pulmonary vein region.   (J Am Coll Cardiol Img 2012;5: 1211–20) © 2012 by the American College of Cardiology Foundation

Chronic atrial fibrillation (AF) remains one of the greatest challenges in cardiac arrhythmia therapy. Despite the high success rate of pulmonary vein (PV) ablation in paroxysmal forms, effective ablation therapy in patients with chronic AF remains elusive (1), due to the still incomplete understanding of the mechanisms sustaining the arrhythmia.

See page 1221

Potential driver sources, characterized by rapid and repetitive activations, as well as areas with fractionated electrograms, have been proposed as critical regions for the maintenance of AF (2–4). The identification and localization of electrograms with these features may improve the success rate of targeted ablation. In order to identify potential AF drivers from single atrial electrograms, a new time-domain approach has been proposed based on the combined analysis of atrial cycle length (CL) and wave similarity (WS) (5). WS analysis is a technique to assess directional organization during fibrillation (6,7), whose performances have been thoroughly tested in previous AF studies (6,8,9). Specifically, WS analysis measures the degree of repetitiveness over time of electrogram activation waveforms, thus allowing the identification of repetitive (R) sources of activation. Complementarily, CL analysis provides a local measure of the fibrillatory rate, determining among organized sources those with the shortest CL.

In the present work, we set out to construct anatomically detailed WS and CL maps to investigate the anatomic distribution of potential drivers in patients with persistent AF. This task was performed by a set of innovative signal and imaging techniques directed to the integration of WS/CL maps with highly resolved 3-dimensional (3D) anatomic reconstructions of the atrial chambers (5,10,11). Accurate 3D computed tomography (CT) reconstructions of the atrial anatomy were obtained by a semiautomatic segmentation process based on a marker-controlled watershed segmentation (11). The spatial distribution of WS/CL indexes was assessed by applying WS analysis and CL measure to each atrial electrogram recorded by an electroanatomic mapping system. Sparse-point WS and CL maps were then integrated on CT atrial

Table 1. Patient and Mapping Characteristics

Age, yrs	58 ± 9
Male, n	12 (60%)
Heart disease, n	15 (75%)
Hypertension, n	5 (25%)
Atrial fibrillation duration, months	19 ± 11
Left atrial diameter, mm	
Parasternal	43 ± 8
Longitudinal	61 ± 7
Mapping time, min	44 ± 8

Values are mean ± SD or n (%).

reconstructions by a fully automated registration and fusion procedure based on a stochastic approach (10).

METHODS

Study patients. Twenty consecutive patients with persistent AF (duration ≥6 months), who underwent catheter ablation for drug-refractory, symptomatic AF, were studied. Patient characteristics are shown in Table 1. The duration of continuous AF was more than 1 year in 18 patients (long-standing persistent AF), whereas in 2 patients, AF lasted 6 and 10 months, respectively. Fifteen of the 20 patients had underlying heart diseases, including 5 patients with hypertensive heart disease. All patients provided written informed consent. The study was approved by the local institution's research ethics board.

Biatrial CT imaging and segmentation. All patients underwent cardiac multidetector CT imaging within 24 h before the ablation procedure. Scans were performed with a 16-slice helical scanner (Philips 8000 Mx IDT, Philips Medical System, Best, the Netherlands) during an inspiratory breath-hold, after intravenous injection of 125 ml of contrast medium (Iomeron 400, Bracco, Italy). Whenever possible, motion artifacts were minimized by retrospective electrocardiogram gating reconstruction at the end-diastolic phase, whereas in patients with high-frequency AF, cardiac gating was not applied.

The isolation of the 3D anatomy of the left atrium (LA), PV, and right atrium (RA) from CT images was performed by a custom-made semiautomatic algorithm based on marker-controlled watershed segmentation. Technical details on the segmentation procedure have been provided elsewhere (11). The 3D reconstructed biatrial surfaces were used in the subsequent registration procedure.

Electrophysiological study and electroanatomic mapping. A quadripolar catheter was placed at the His position and a 20-pole deflectable catheter was

inserted into the coronary sinus (CS) for continuous monitoring. Real-time 3D left and right atrial maps were reconstructed by an electroanatomic mapping system (CARTO XP, Biosense Webster, Inc., Diamond Bar, California), sampling evenly distributed endocardial sites with a fill-threshold of 15 to 20 mm. The catheter (NAVISTAR THERMOCOOL, Biosense Webster, Inc.) was held stationary in each location, allowing the acquisition of a bipolar endocardial electrogram of 10-s length at each site. Atrial bipolar electrograms, surface electrocardiograms, and CS signals were continuously monitored and stored on a computer-based digital amplifier/recorder system (C.R. Bard Inc., Bard Electrophysiology Division, Lowell, Massachusetts). Intracardiac electrograms were band-pass filtered (30 to 500 Hz) and digitized at 1-kHz sampling frequency. All electrograms were exported for off-line measurement and analysis. Electrograms presenting an unsatisfying signal-to-noise ratio were excluded from subsequent analysis.

Measurement of CL and WS. The 10-s bipolar electrograms recorded at each mapped location were analyzed to obtain local measures of CL and WS.

For CL measurement (5), bipolar electrograms were first pre-processed to remove ventricular interference by an averaging technique. Local atrial activation waves were then identified by signal filtering and comparison with an adaptive threshold, accounting for variations in waveform amplitude. Following wave recognition, atrial activation times were estimated by measuring the barycenter of local activation waves, defined as the time that divided into 2 equal parts the local area of the modulus of the signal. The method provided a reliable estimation of activation times even in presence of fragmented potentials and complex wave morphologies, since the barycenter was computed from the whole shape of the activation wave and thus was less sensitive to local modifications of the waveform (5).

The degree of repetitiveness of the fibrillatory process at each recording site was quantified by measuring the level of similarity of the activation waves (similarity index [S]) (6). S was determined by comparing the morphologies of all possible pairs of atrial activation waves extracted from a single recording. Details on the calculation of S, as well as on its performance in the determination of the
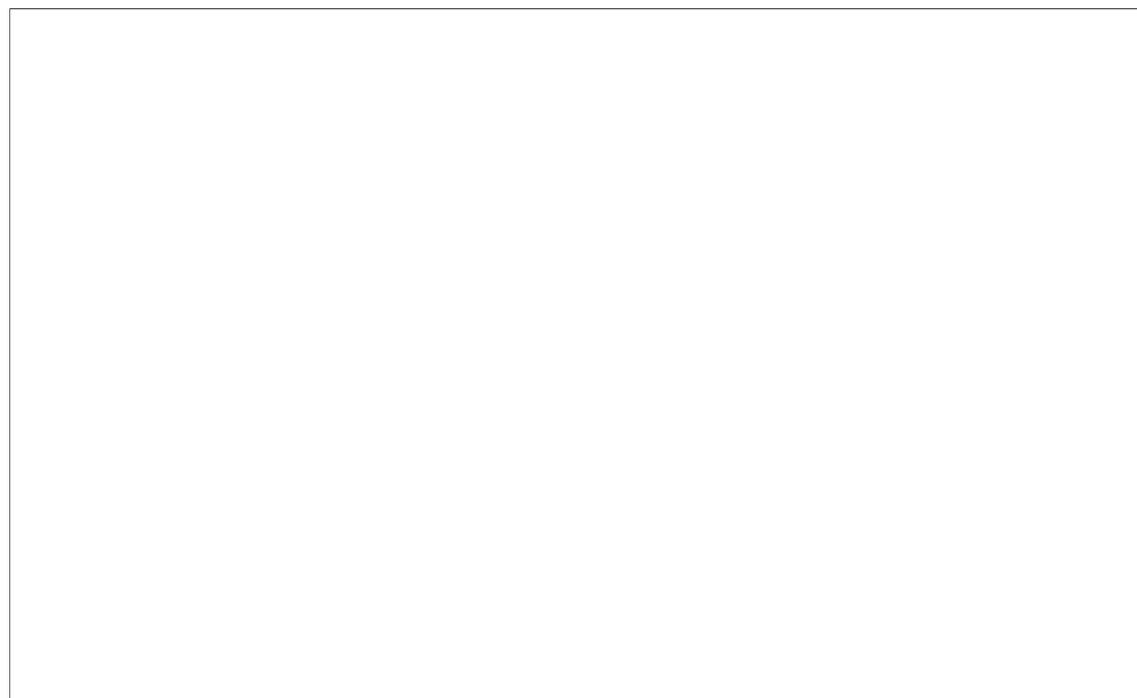
Figure 1. Construction of Anatomically Detailed WS Maps

(A) Registration of mapping points on the 3-dimensional (3D) computed tomography (CT)-reconstructed biatrial endocardial surface and evaluation of the similarity index (S). On the **right**, bipolar signals recorded during persistent atrial fibrillation (AF) at 5 different locations of the atria, and corresponding S values obtained by wave superimposition and quantitative comparison. Note that electrograms with regular and repetitive activation waveforms yield high-similarity values (S = 0.99, **site a**), whereas the index significantly decreases for fragmented signals (S = 0.14, **site e**). **(B)** Application of wave similarity (WS) analysis to the whole set of mapping points and fusion of similarity values on the biatrial surface. Similarity values are color coded, with **blue** indicating high-similarity and **red** low-similarity values.

spatiotemporal complexity of AF have been published elsewhere (6,8,9). Figure 1A shows representative examples of the application of WS analysis to bipolar electrograms recorded at different atrial sites and presenting various degree of morphological complexity.

The temporal stability of WS/CL indexes was checked by analyzing the CS electrograms over the entire duration of the mapping study. No significant variations were observed either in S (S = 0.21 ± 0.13 vs. 0.21 ± 0.14 vs. 0.21 ± 0.11; p = NS) nor in CL (CL = 169.7 ± 18.8 ms vs. 165.8 ± 21.8 ms vs. 165.6 ± 20.0 ms; p = NS) between the beginning, middle, and end of the study.

Integration and fusion of WS/CL maps with biatrial CT images. Anatomically detailed WS/CL maps were constructed by determining S and CL indexes at each mapping site, and subsequently, registering mapping points and fusing the corresponding indexes on LA and RA anatomic reconstructions (Fig. 1). The registration step was performed by a custom-made, landmark-free algorithm, based on a stochastic approach, which has been detailed elsewhere (10). Briefly, a parameterized rigid geometric transformation was repeatedly applied to the map-

ping points, searching for the best parameter set that minimized the misalignment between transformed points and atrial reconstructions. The stochastic procedure was fully automated and proved accurate and reproducible data integration (10). Following registration, WS/CL values associated with the mapping points were fused on the registered 3D CT atrial surfaces by a radial basis function interpolation.

After the construction of WS/CL maps, a detailed spatial analysis was performed to evaluate the presence of regional index differences. The RA was divided into superior caval vein (SCV) and anterior, lateral, posterior, and septal regions, whereas the LA was separated into the 4 pulmonary veins (PVs) and posterior wall, septum, roof, and appendage regions.

Statistical analysis. Continuous data are presented as mean ± SD, and categorical data as numbers or percentages. One-way analysis of variance for repeated measures was performed to compare S/CL values among atrial regions, followed by post hoc analysis with Bonferroni correction. Variable normality distribution was evaluated by Shapiro-Wilk test. A p value <0.05 was considered statistically significant. Statistical analysis was performed with
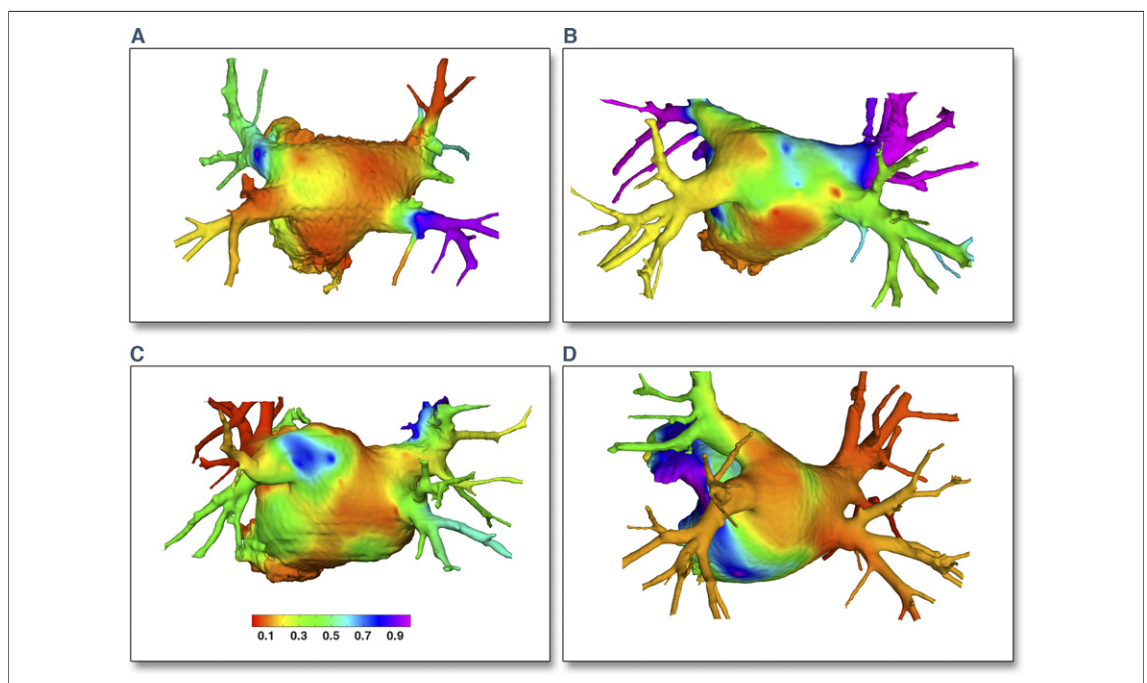
Figure 2. Anatomical Distribution of WS During Persistent AF in the LA of 4 Different Patients

The values of the similarity index (S) are color coded, with **blue** indicating high-similarity and **red** low-similarity values. Repetitive (R) sources were defined as region with S ≥0.5. Patient in **A** displays R sources at the left superior and right inferior pulmonary veins (PVs), whereas patient **B** at both right and left superior PVs. Patient in **C** shows R sources at the ostium of the left PV common trunk and on the anterior wall of the right superior PV. Differently, in patient **D**, all PVs are highly disorganized, whereas a wide high-similarity region is present at the left atrial appendage. LA = left atrium; other abbreviations as in Figure 1.
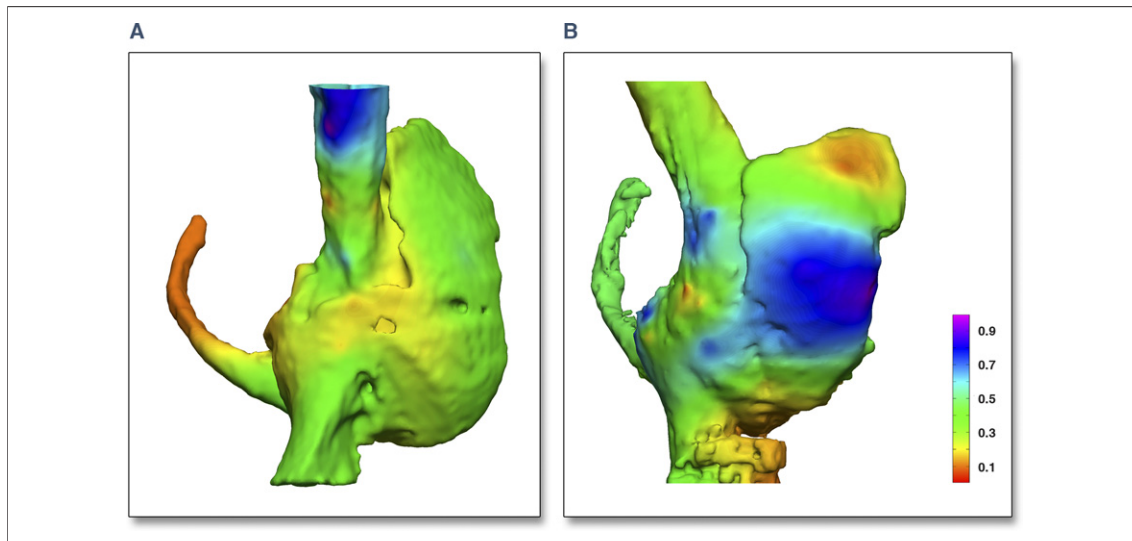
Figure 3. Anatomic Distribution of WS During Persistent AF in the RA of 2 Different Patients

The values of the similarity index are color coded with **blue** indicating high-similarity and red low-similarity values. Repetitive (R) sources were defined as region with S ≥0.5. Note the localization of R sources at the superior caval vein **(A)** and on the lateral wall **(B)**. RA = right atrium; other abbreviations as in Figure 1.

Origin 8.1 Pro (OriginLab Corporation, North-ampton, Massachusetts).

RESULTS

WS/CL mapping and registration. To construct WS/CL biatrial maps 123 ± 14 mapping points per patient were acquired (47 ± 6 in the RA and 76 ± 14 points in the LA, respectively). Map analysis was accomplished in 17 patients. Three patients were excluded due to the high number of electrograms with poor signal-to-noise ratio.

In all patients, RA/LA electroanatomic maps were successfully registered on the corresponding 3D CT surface reconstructions with good accuracy (mean point-to-surface distance of 2.37 ± 0.68 mm and 2.22 ± 0.44 mm for RA and LA, respectively) and precision (point scattering over 20 parallel solutions of 1.57 ± 0.48 mm and 1.43 ± 0.75 mm for RA and LA, respectively).

Anatomic distribution of WS. Regional analysis of fused wave similarity maps showed the existence of clear regional differences in wave similarity in both left and right atria (Figs. 2 and 3). On average (Fig. 4), regions with highly organized electrical activity (high-similarity indexes) were found in the PVs (S = 0.46 ± 0.13) and LA appendage (S = 0.43 ± 0.19), whereas disorganized areas, charac-terized by low-similarity values, were located on the posterior wall, roof, and septum (S = 0.17 ± 0.08). Focusing on the PV region, the levels of similarity

were slightly higher at the superior than the inferior PVs (S = 0.49 ± 0.15 vs. S = 0.42 ± 0.16, p = NS) and at the distal portion of the veins than around the ostium (S = 0.47 ± 0.14 vs. S = 0.31 ± 0.15, p<0.001). In the RA, high-similarity values were found at the SCV (S = 0.47 ± 0.18) and on the anterior wall (S = 0.42 ± 0.13), whereas posterior and septal regions were the most disorga-nized sites (S = 0.27 ± 0.10).

Anatomic distribution of R sources. In each patient, regions showing S ≥0.5 were selected and marked as repetitive (R) sources. The regional distribution of R sources for the whole population of patients is shown in Figure 4. In 17 patients, a total of 49 R sources were found, with an average of 2.9 ± 1.6 sources per patient (range 0 to 6). R sources were present in almost all patients (94%) and were mainly located in the LA (35 of 49). As evidenced by the representative examples of Figure 2 and by the cumulative data in Figure 4, R sources in the LA were exclusively present at the PV level (31 sources in 82% of patients) and LA appendage (4 in 23% of patients). Focusing on the 4 PVs, the incidence of repetitive activity was higher at the superior than the inferior PVs (18 vs 13). R sources on the RA (Figs. 3 and 4) were mostly located at the SCV (7 of 14) and on the anterior walls (4 of 14).

Anatomic distribution of CL. Map fusion and re-gional analysis were performed also for atrial CLs.
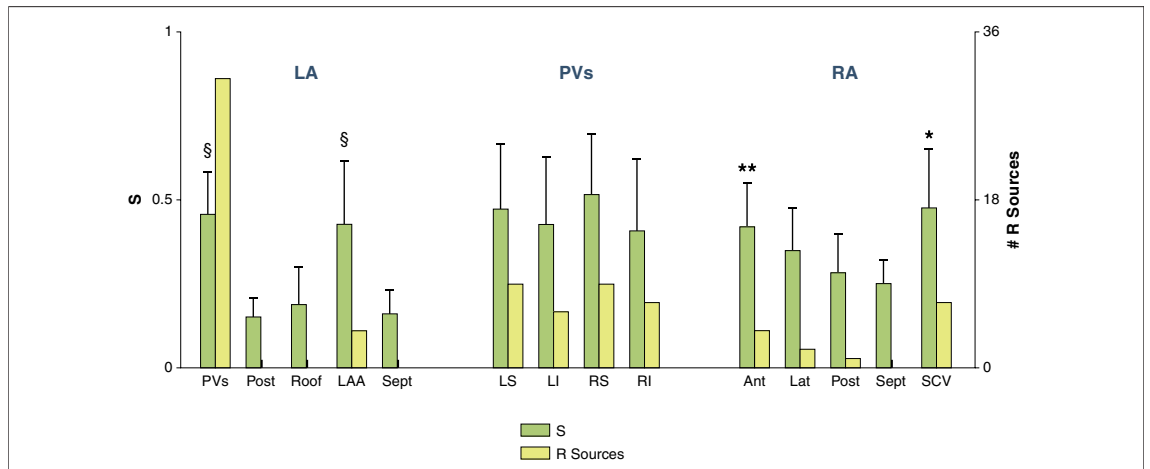
Figure 4. Regional Distribution of WS and R Sources in Persistent AF Patients

Mean similarity index (S) and number of repetitive sources (R sources) are displayed for different atrial regions. §p < 0.001 compared with LA Post, Roof, and Sept; *p < 0.05, **p < 0.01 compared with RA Lat, Post, and Sept. Ant = anterior wall; LAA = left atrial appendage; Lat = lateral wall; LI = left inferior pulmonary vein; LS = left superior pulmonary vein; Post = posterior wall; RI = right inferior pulmonary vein; RS = right superior pulmonary vein; SCV = superior caval vein; Sept = septum; other abbreviations as in Figures 1, 2, and 3.

The mean atrial CLs calculated in each atrial region are shown in Table 2. On average, the LA showed a faster rate than the RA (CL = 164.2 ± 20.0 ms vs. 169.9 ± 20.9 ms, p < 0.05). No significant difference in CL was observed among different LA regions (p = NS). The average PV CL was 166.2 ± 24.1 ms, with shorter cycles around the ostium than in the distal area (163.2 ± 23.0 ms vs. 168.7 ± 25.8
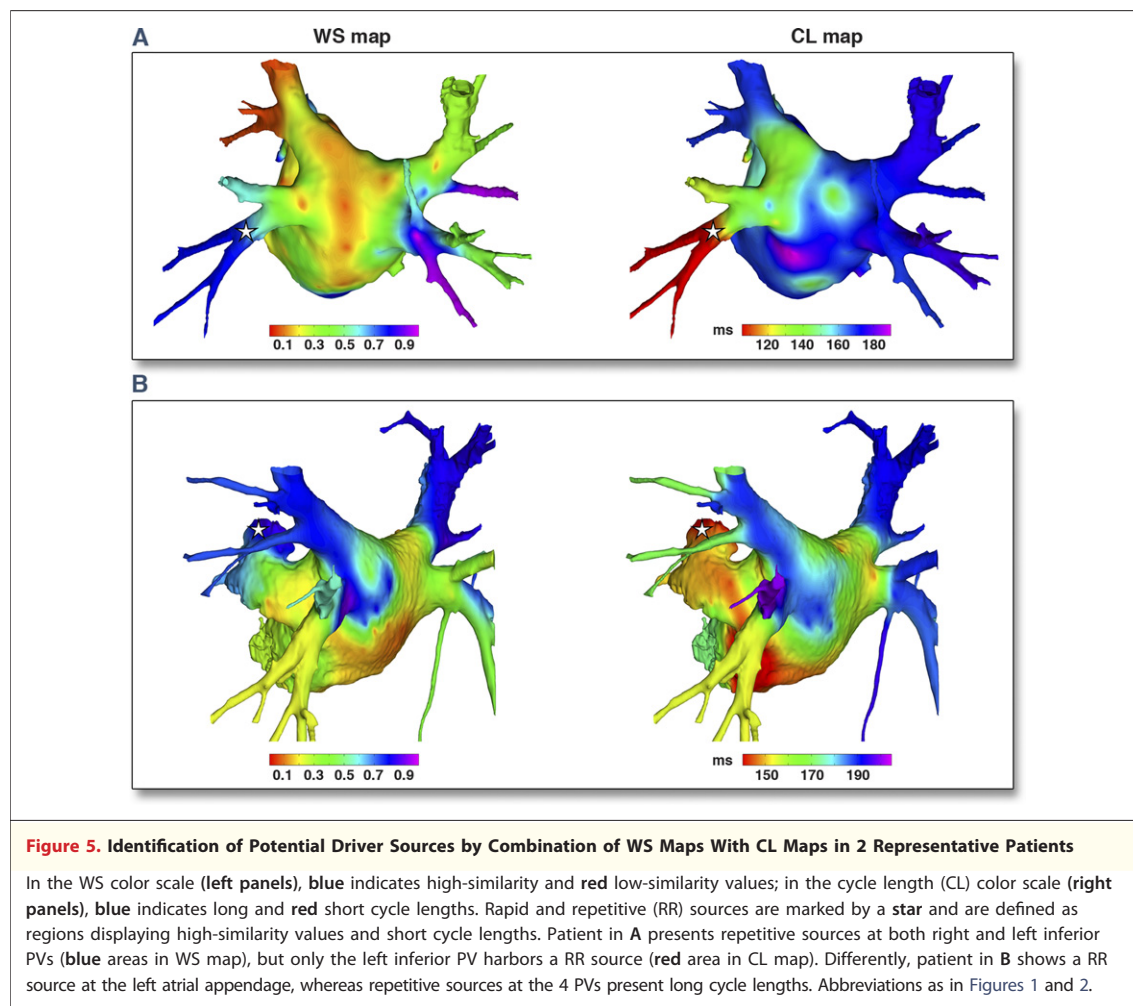
ms, p < 0.01). Regional CL differences were observed in the RA (p < 0.01), where the SCV showed the slowest atrial rate (CL = 184.7 ± 14.6 ms, p < 0.01).

Anatomic distribution of RR sources. To identify among R sources those showing a rapid rate, WS maps were systematically compared with CL maps in each patient (Fig. 5). Regions displaying electrical activity with high similarity (S ≥0.5) and high rate of activation (CL < CL of the surrounding tissue) were selected and marked as rapid and repetitive (RR) sources. Only the 33% of the R sources (16 of 49) showed a high activation rate and were thus classified as potential drivers (S = 0.65 ± 0.15; CL = 140.7 ± 25.1 ms, range 104 to 188 ms). As detailed in Table 3, RR sources were present in 11 of 17 patients (65%) and were mainly confined to the LA (12 of 16 sources) at the level of PVs (10 sources) and LA appendage (2 sources) (see example in Fig. 5), whereas they were rarely found in the RA. Focusing on the 4 PVs, the highest incidence of drivers was found at the left superior PV (4 of 10), whereas the right inferior showed the lowest incidence (1 of 10). PV drivers were mostly located at the proximal portion of the veins rather than at the distal area (6 vs. 4). Interestingly (Fig. 6), although the majority of patients (82%) showed R sources in the PVs, R sources displayed the fastest rate in just half of the patients (47%). More importantly, the SCV, which presented highly repetitive activity in 7 of 17 patients (41%), displayed a rapid rate just in 1 patient.

Table 2. Regional Distribution of Atrial CL During Persistent AF

Location	CL (ms)
PVs	
LS	165.7 ± 26.8
LI	160.5 ± 22.9
RS	170.9 ± 25.6
RI	169.2 ± 29.0
LA	
Post	164.3 ± 15.6
Roof	161.2 ± 19.3
Sept	168.3 ± 24.3
LAA	162.7 ± 25.3
RA	
Ant	162.2 ± 25.5
Lat	163.2 ± 28.3
Post	170.6 ± 23.0
Sept	168.6 ± 20.5
SCV	184.7 ± 14.6*

Values are mean ± SD. *p < 0.01 compared with all other RA regions.
Ant = anterior wall; CL = cycle length; LA = left atrium; LAA = left atrial appendage; Lat = lateral wall; LI = left inferior; LS = left superior; Post = posterior wall; PV = pulmonary vein; RA = right atrium; RI = right inferior; RS = right superior; SCV = superior caval vein; Sept = septum.

Figure 5. **Identification of Potential Driver Sources by Combination of WS Maps With CL Maps in 2 Representative Patients**

In the WS color scale (**left panels**), **blue** indicates high-similarity and **red** low-similarity values; in the cycle length (CL) color scale (**right panels**), **blue** indicates long and **red** short cycle lengths. Rapid and repetitive (RR) sources are marked by a **star** and are defined as regions displaying high-similarity values and short cycle lengths. Patient in **A** presents repetitive sources at both right and left inferior PVs (**blue** areas in WS map), but only the left inferior PV harbors a RR source (**red** area in CL map). Differently, patient in **B** shows a RR source at the left atrial appendage, whereas repetitive sources at the 4 PVs present long cycle lengths. Abbreviations as in Figures 1 and 2.

DISCUSSION

Localization of AF critical sources by anatomically detailed WS/CL maps. This paper introduces a novel strategy for the identification and localization of potential AF drivers, based on the construction of anatomically detailed WS/CL maps. Advanced signal analysis and image processing techniques were combined to extract and quantify the principal electrophysiological features of mapping electrograms, and integrate the electrophysiological information with the highly detailed atrial anatomy provided by CT images.

Previous experimental evidence has pointed out AF drivers to be characterized by 2 principal features, which are a fast activation rate and a high level of electrical organization (12,13). A novel time-domain approach was used to translate this electrophysiological definition into an operative definition of driver, based on quantitative signal properties. Specifically, critical sites were identified

by a double-criteria evaluation, which combined a measure of WS with a measure of CL. As shown in a preliminary methodological study (5), the combined evaluation of the 2 indexes conferred to the method a high sensitivity to distinguish potential driver sites from substrate or passive activation regions.

Following identification, AF drivers were localized in a highly detailed anatomic context by integrating the sparse WS/CL maps with CT-derived anatomies via custom-made image processing algorithms (10,11). Integration of multimodal data was aimed to overcome the coarse anatomic detail of the reconstructed map provided by electroanatomic mapping systems. The LA anatomy is indeed complex, and high inter- and intrapatient variability is observed in the number, size, and bifurcation of the PVs (14). Complex anatomic structures cannot be reconstructed from raw mapping data, whereas an accurate description of these aspects can be derived from CT images (15). In the

1218   Ravelli *et al.*
Localization of Driver Sources in AF

J A C C :   C A R D I O V A S C U L A R   I M A G I N G ,   V O L .   5 ,   N O .   1 2 ,   2 0 1 2
D E C E M B E R   2 0 1 2 : 1 2 1 1 – 2 0

Table 3. Characteristics of RR Sources in Persistent AF Patients

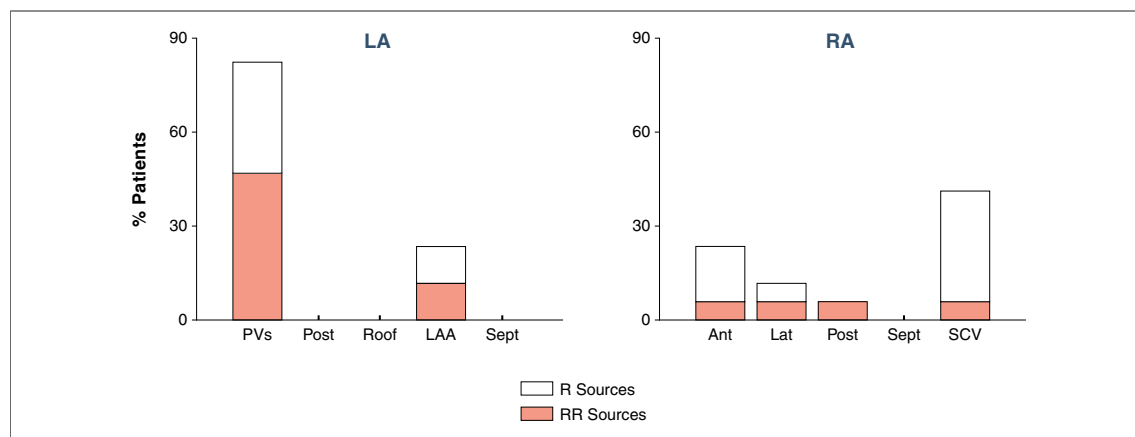| Patient #	Sources, n	Location	CL (ms)	S
1	1	LIPV prox	145	0.55
2	2	LSPV dist	145	0.52
		RA Post	148	0.53
3	0	—	—	—
4	1	SCV prox	188	0.73
5	2	LIPV prox	180	0.63
		RSPV prox	186	0.81
6	1	PV LCT prox	124	0.52
7	0	—	—	—
8	0	—	—	—
9	1	LIPV dist	104	0.79
10	1	LAA	136	0.85
11	1	LSPV prox	123	0.57
12	2	RSPV prox	122	0.52
		RIPV dist	130	0.98
13	3	LAA	121	0.78
		RA Ant	124	0.53
		RA Lat	123	0.54
14	0	—	—	—
15	0	—	—	—
16	1	LSPV dist	152	0.55
17	0	—	—	—

Cycle length (CL) and similarity index (S) refer to the site with the shortest cycle length in the rapid repetitive region. dist = distal; LCT = left common trunk; LIPV = left inferior pulmonary vein; LSPV = left superior pulmonary vein; prox = proximal; RIPV = right inferior pulmonary vein; RR = rapid and repetitive; RSPV = right superior pulmonary vein; other abbreviations as in Table 2.

AF critical sites, providing a detailed picture of their anatomic distribution in the LA and inside the complex branching structure of the PVs. The accuracy in driver localization was obtained by innovative custom-made algorithms of proved efficiency (10,11), which allowed both a highly resolved reconstruction of the atrial chambers from CT data (11) and an accurate registration and fusion of multimodal data (10). In particular, our landmark-free, fully automated stochastic approach enabled the registration of mapping points on CT reconstructions with accuracy suitable for the detection of regional differences in the WS/CL indexes.

Anatomic distribution of potential drivers in persistent AF. The combined use of CT-integrated WS/CL maps allowed us to demonstrate the presence of clear regional differences in the distribution of potential drivers in patients with persistent AF. Consistent with experimental studies (12,13), high-frequency R sources were not uniformly distributed, but were prevalently confined to the LA and, specifically, to the PV and LA appendage regions. The spatial location of these potential drivers is also in agreement with high-density epicardial mapping studies performed in patients with chronic AF during open heart surgery (16–21). High-frequency repetitive patterns emerging from the posterior LA at or near the PVs, associated with foci or re-entrant circuits, were reported by several authors (16,18,19,21). In a few of these studies, targeted LA ablation at these sites was successfully applied, suggesting the important role of repetitive activation in the perpetuation of chronic AF (16–18).

Our results showed the confinement of potential driver sources in the LA, whereas organized sources

context of AF ablation, integration of electroanatomic data with tomographic images is performed to facilitate the procedure and has been shown to improve ablation outcome (15). In the present paper, the construction of CT-integrated WS/CL maps allowed us to precisely locate the position of

Figure 6. Incidence of RR Sources in Persistent AF Patients in the LA and RA Regions

Colored bars indicate the percentage of patients with rapid and repetitive (RR) sources, whereas **white bars** correspond to the percentage of patients with sole repetitive (R) sources. Abbreviations as in Figures 1, 2, 3, and 4.

in the RA were rarely associated with high-frequency activation. The incidence of AF drivers observed in the PV region (47% of patients) is consistent with the modest outcome of PV ablation in persistent/long-standing persistent AF with respect to paroxysmal AF (1,22). Similarly, the paucity of drivers observed in the RA is in agreement with the secondary role of RA ablation and/or SCV isolation procedures, which were shown to be adjuvant only in a limited subgroup of patients (23).

In this study, we identified other atrial regions with highly repetitive electrical activity but with slow activation rates. A significant example is represented by the SCV. The combination of a high level of organization and a slow activation may indicate the presence of a passively activated region or a secondary source of activation.

Finally, the construction of WS maps provided indications on the spatial distribution of complex fractionated electrograms, identified by low-similarity values. Complex electrogram areas were localized on the posterior wall, roof, and septum of the LA, and on the posterior wall and septum of the RA, which is in agreement with the distribution of fragmented electrograms firstly described by Nademanee et al. (4) and confirmed by several subsequent studies.

Study limitations. The optimal gold standard for the identification of AF critical sources would be targeted ablation. However, due to the retrospective nature of our study, the effects of targeted ablation on the identified driver sites could not be determined. Nonetheless, our work showed the possibility of objectively identifying and precisely localizing regions of rapid and repetitive activity, which have been previously demonstrated to maintain AF.

Also, regions with RR sources identified by our approach coincided with potential driver regions identified by other ablation studies (16–18). Our study may thus represent the base for planning future targeted ablations proving the actual role of these areas in AF maintenance.

Other limitations consisted of the evaluation of WS/CL temporal stability on the sole continuous CS recordings and in the off-line analysis of electrograms and images. However, it is worth noticing that the spatiotemporal stability of the 2 indexes during AF has been demonstrated in previous studies (8,9), and the low computational cost of the algorithms is consistent with future online implementation.

CONCLUSIONS

The identification and localization of RR sources in AF patients is feasible by fusion of biatrial anatomic images with WS/CL maps. R sources of rapid impulse are present in a subset of patients with persistent AF and are mainly localized in the region of the PVs and LA appendage. The combined use of anatomically integrated WS/CL maps, which allows the detection of 2 critical features of AF sources, may constitute a novel mapping modality for the electrogram-guided ablation of AF.

REFERENCES

1. Matsuo S, Lim KT, Haissaguerre M. Ablation of chronic atrial fibrillation. Heart Rhythm 2007;4:1461–3.

2. Sanders P, Berenfeld O, Hocini M, et al. Spectral analysis identifies sites of high-frequency activity maintaining atrial fibrillation in humans. Circulation 2005;112:789–97.

3. Atienza F, Jalife J. Reentry and atrial fibrillation. Heart Rhythm 2007;4:S13–6.

4. Nademanee K, Lockwood E, Oketani N, Gidney B. Catheter ablation of atrial fibrillation guided by complex fractionated atrial electrogram mapping of atrial fibrillation substrate. J Cardiol 2010;55:1–12.

5. Ravelli F, Masè M. A time-domain approach for the identification of atrial fibrillation drivers. Conf Proc IEEE Eng Med Biol Soc 2011;2011:5527–30.

6. Faes L, Nollo G, Antolini R, Gaita F, Ravelli F. A method for quantifying atrial fibrillation organization based on wave morphology similarity. IEEE Trans Biomed Eng 2002;49:1504–13.

7. Masse S, Downar E, Chauhan V, Sevaptsidis E, Nanthakumar K. Wave similarity of human ventricular fibrillation from bipolar electrograms. Europace 2007;9:10–9.

8. Ravelli F, Faes L, Sandrini L, et al. Wave similarity mapping shows the spatiotemporal distribution of fibrillatory wave complexity in the human right atrium during paroxysmal and chronic atrial fibrillation. J Cardiovasc Electrophysiol 2005;16:1071–6.

9. Ravelli F, Masè M, Del Greco M, Faes L, Disertori M. Deterioration of organization in the first minutes of atrial fibrillation: a beat-to-beat analysis of cycle length and wave similarity. J Cardiovasc Electrophysiol 2007;18:60–5.

10. Cristoforetti A, Masè M, Faes L, et al. A stochastic approach for automatic registration and fusion of left atrial electroanatomic maps with 3D CT anatomical images. Phys Med Biol 2007;52:6323–37.

11. Cristoforetti A, Faes L, Ravelli F, et al. Isolation of the left atrial surface from cardiac multi-detector CT images based on marker controlled watershed segmentation. Med Eng Phys 2008;30:48–58.

12. Mandapati R, Skanes A, Chen J, Berenfeld O, Jalife J. Stable microreentrant sources as a mechanism of atrial fibrillation in the isolated sheep heart. Circulation 2000;101:194–9.

13. Kalifa J, Tanaka K, Zaitsev AV, et al. Mechanisms of wave fractionation at boundaries of high-frequency excitation in the posterior left atrium of the isolated sheep heart during atrial fibrillation. Circulation 2006;113:626–33.

14. Ho SY, Cabrera JA, Tran VH, Farre J, Anderson RH, Sanchez-Quintana D. Architecture of the pulmonary veins: relevance to radiofrequency ablation. Heart 2001;86:265–70.

15. Tops LF, Schalij MJ, den Uijl DW, Abraham TP, Calkins H, Bax JJ. Image integration in catheter ablation of atrial fibrillation. Europace 2008;10 Suppl 3:iii48–56.

16. Harada A, Konishi T, Fukata M, Higuchi K, Sugimoto T, Sasaki K. Intraoperative map guided operation for atrial fibrillation due to mitral valve disease. Ann Thorac Surg 2000;69:446–50.

17. Sueda T, Imai K, Ishii O, Orihashi K, Watari M, Okada K. Efficacy of pulmonary vein isolation for the elimination of chronic atrial fibrillation in cardiac valvular surgery. Ann Thorac Surg 2001;71:1189–93.

18. Yamauchi S, Ogasawara H, Saji Y, Bessho R, Miyagi Y, Fujii M. Efficacy of intraoperative mapping to optimize the surgical ablation of atrial fibrillation in cardiac surgery. Ann Thorac Surg 2002;74:450–7.

19. Wu TJ, Doshi RN, Huang HL, et al. Simultaneous biatrial computerized mapping during permanent atrial fibrillation in patients with organic heart disease. J Cardiovasc Electrophysiol 2002;13:571–7.

20. Sahadevan J, Ryu K, Peltz L, et al. Epicardial mapping of chronic atrial fibrillation in patients: preliminary observations. Circulation 2004;110:3293–9.

21. Nitta T, Ishii Y, Miyagi Y, Ohmori H, Sakamoto S, Tanaka S. Concurrent multiple left atrial focal activations with fibrillatory conduction and right atrial focal or reentrant activation as the mechanism in atrial fibrillation. J Thorac Cardiovasc Surg 2004;127:770–8.

22. Tilz RR, Chun KR, Schmidt B, et al. Catheter ablation of long-standing persistent atrial fibrillation: a lesson from circumferential pulmonary vein isolation. J Cardiovasc Electrophysiol 2010;21:1085–93.

23. Oral H, Chugh A, Good E, et al. Randomized evaluation of right atrial ablation after left atrial ablation of complex fractionated atrial electrograms for long-lasting persistent atrial fibrillation. Circ Arrhythm Electrophysiol 2008;1:6–13.